SCIENCE CHINA
Chemistry

• ARTICLES •

June 2013 Vol.56 No.6: 763–772
doi: 10.1007/s11426-012-4828-y

Thermodynamics of glycerol hydrogenolysis to propanediols over supported copper clusters: Insights from first-principles study

GUAN Jing, WANG XiCheng, WANG XiaoYan & MU XinDong*

Key Laboratory of Biofuels, Qingdao Institute of Bioenergy and Bioprocess Technology, Chinese Academy of Sciences, Qingdao 266101, China

Received October 25, 2012; accepted December 10, 2012; published online January 21, 2013

Copper catalysts supported on metal oxides display unique efficiency and selectivity in catalyzing glycerol hydrogenolysis to propanediols. Understanding the reaction at the molecular level is the key to rational design of better catalysts for propanediol synthesis, which is one of the major challenges for glycerol application in energy. In this work, extensive calculations based on periodic density functional theory were carried out to study thermodynamics of glycerol hydrogenolysis over binary model catalysts, including Cu/ZrO_2 and Cu/MgO, with the focus to elucidate the competitive reaction pathways to produce the 1,2-propanediol (1,2-PDO) and 1,3-propanediol (1,3-PDO). Our results suggest that the reaction starts with glycerol dehydration on the metal oxide, followed by sequential hydrogenation over metal centers. Based on our explorations on the stabilities of adsorbed reactants, dehydrated intermediates and hydrogenated species along the reaction channels, the DFT calculations show that the 1,2-PDO formation will dominate in comparison to the 1,3-PDO from thermodynamic viewpoint. This is consistent with our experiments where the Cu catalysts seem to give the 1,2-PDO as a main product. The calculations and experiments also indicate that the Cu/MgO exhibits superior activities than Cu/ZrO_2 for the hydrogenolysis of glycerol molecules.

density functional calculations, glycerol hydrogenolysis, propanediols, copper-based catalysts, mechanism

1 Introduction

Catalytic conversion of renewable feedstock and chemicals is attracting considerable interest in terms of green chemistry. Glycerol has been regarded as one of the top-12 building block chemicals that can be derived from sugar and converted to high value-added bio-based chemicals or materials [1]. In addition, it is the main by-product in the biodiesel production by transesterification of vegetable oils and animal fats [2]. Therefore, using the growing supply of glycerol is a highly profiting step in moving toward a more sustainable economy.

Until now, a great deal of effort has been put toward the utilization of glycerol. One of the attractive outlets of glycerol is to produce glycols, especially propanediols, by an alternative route involving selective hydrogenolysis of glycerol. Various catalysts have been extensively attempted for this reaction. A bifunctional system was typically used which was composed of acid or base support and hydrogenation catalyst such as Cu, Ni, Ru, Rh and Pt [3–10]. The composition of metals and the nature of the oxidic supports were found to influence the ability of the catalysts to both activate the glycerol substrate and selectively convert it to propanediol. The copper-based catalysts were found to exhibit superior performance in the hydrogenolysis reaction due to their high efficiency for C–O bond cleavage and poor activity for C–C bond breaking [11]. The predominant product in most cases was 1,2-propanediol (1,2-PDO), whereas the production of 1,3-propanediol (1,3-PDO) was much lower. Under acidic conditions, the conversion of glycerol was found to be linearly correlated to the number of acid sites on the solid acid [12].The use of ZrO_2 support exhibits good selectivity to propanediols than the more-

*Corresponding author (email: muxd@qibebt.ac.cn)

acidic oxidic supports due to the optimum acidity of this catalytic material. Increased acidity improves activity, but results in poor selectivity due to excessive hydrogenolysis of 1,2-PDO to propanols. Choosing solid base as a component of metal catalyst would be an alternative of the solid acid support. In previous work, it was reported that the alkaline support MgO showed the predominant activity and higher 1,2-PDO selectivity than that of solid acids (Al_2O_3 and zeolites) in Pt-catalyzed hydrogenolysis of glycerol [13]. More recently, it was found that MgO supported copper is also an efficient catalyst for glycerol hydrogenolysis with extraordinary selectivity (97.6%) of 1,2-PDO [6]. In the present work, ZrO_2 and MgO have been selected with the efforts to understand the origin of oxidic support effects on the reactivity of the copper-based catalyst in glycerol hydrogenolysis.

Previous experimental research suggested that the mechanism of glycerol hydrogenolysis to propanediols varied in different reaction media. In acidic conditions, conversion of glycerol proceeds by combination of dehydration of glycerol to acetol (pathway I) /3-hydroxypropanal (pathway II) over acid active sites and consecutive hydrogenation over metal particles (Scheme 1) [3, 5, 8, 10, 14]. This mechanism was supported by identification of acetol in the reaction mixture of glycerol and sugar [15, 16]. According to the above mechanism, the solid acidic support plays a major role in this reaction. Another mechanism proposed by Montassier [17, 18] involves dehydrogenation of glycerol to glyceraldehyde followed by dehydration to 2-hydroxyacrolein and subsequent hydrogenation to 1,2-propanediol with a Ru/C catalyst under neutral/slightly basic aqueous solutions (pathway III, Scheme 1). Thus, the selective conversion of glycerol to propanediols is known as a bifunctional reaction which requires catalysts both for dehydration and for hydrogenation functionality.

While the experimental studies have provided some insights into the reaction pathways, the molecular understanding of the catalytic mechanisms is essential. Theoretical modelling has already proven to be a useful complementary tool to experiments for a better interpretation into the fundamental processes during chemical transformations [19–22]. Up to now, most recent studies have focused on the adsorption and reactivity of glycerol over pure metallic surfaces. The decomposition pathways of glycerol on Pt (111) and Rh (111) surfaces via dehydrogenation or C–C bond scission have been examined with periodic density functional theory (DFT) calculations and the most likely reaction pathways for conversion of glycerol to synthesis gas were established [23–25]. Coll *et al.* presented the thermodynamic profiles regarding the adsorption of glycerol and its dehydration intermediates at the surfaces of Ni (111), Rh (111) and Pd (111) from first principles calculations to identify the key points that control the selectivity of the hydrogenolysis reaction [26]. Likewise, the elementary reactions for glycerol conversion into 1,2-PDO catalyzed by Rh (111) surface were calculated in the framework of DFT approach, which pointed out that dehydrogenation of glycerol into glyceraldehyde was the first step for the glycerol transformation on the Rh/C catalyst in basic media [25, 27].

However, to the best of our knowledge, the reaction mechanism of glycerol hydrogenolysis over supported metal catalysts has never been investigated from a theoretical point of view and the role of oxidic support remains elusive. Herein, in this study, we report on a DFT study on the key steps in the glycerol hydrogenolysis mechanism over copper-based catalysts, aiming to gain a better understanding of two important issues: (i) competitive reaction routes to generate 1,2-PDO and 1,3-PDO, and (ii) the effect of support on the activity. Two common types of metal oxides, namely, ZrO_2 and MgO were considered. The dehydration-hydrogenation mechanism has been proposed for copper-based catalysts. The stability and reaction energetics of the adsorbed reactants, dehydrated intermediates and hydrogenated species were explored. Then the results from DFT calculations can be compared with the experimental reactivity trends. This work can be extended to provide a consistent description of a class of bifunctional heterogeneous catalysts, based on the combination of acid supports and metals for the C–O hydrogenolysis of glycerol.

2 Methods and models

2.1 Computational methods

Plane-wave DFT calculations with the projector-augmented wave (PAW) method were carried out as implemented in

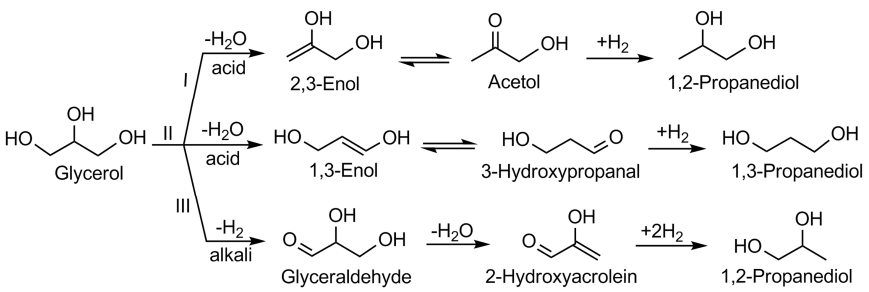

Scheme 1 Schematic reaction pathways (I, II and III) of glycerol hydrogenolysis to form propanediols.

the Vienna ab initio Simulation package (VASP) [28–31]. The generalized gradient approximation with the Perdew-Wang exchange-correlation functional (GGA-PW91) was used [32], which has been shown to work well for surfaces. The kinetic energy cutoff for a plane wave basis set was 400 eV. We applied Monkhorst-Pack mesh *k*-points [33] of (3 × 3 × 3) and (3 × 3 × 1) for bulk and surface calculations which ensures the convergence of the whole system. Structural optimization was based on the conjugate gradient-minimization scheme and the spin unrestricted calculations were also performed. The convergence of energy and forces were set to 1×10^{-4} eV and 0.03 eV/Å, respectively.

2.2 Surface models

The Cu_4 clusters were chosen since it was the smallest three-dimensional structure that provided both metal-metal and metal-support interactions [34–38]. Similar cluster models have been utilized for Cu nanoparticles deposited on CeO_2 and Al_2O_3 supports and shown to be able to capture the chemistry of nanosized metal particles in catalytic reactions [34, 38]. In order to investigate the effect of copper cluster size on the adsorption and energetics of glycerol and intermediates, a larger Cu_8 cluster was constructed. We adopted the cubic ZrO_2 model in the present calculations, which is the stable polymorph of pure ZrO_2 only at temperatures above 2650 K and up to the melting point at 2950 K. At lower temperatures, the stable phases are tetragonal (from 1400 to 2650 K) and monoclinic (up to 1400 K). The cubic structure can be stabilized by doping with lower-valence cations, and this is, in fact, the phase present in many catalytic applications [39]. It has also been shown that zirconia thin films grown on Pt (111) present a cubic structure [40]. Furthermore, the XRD patterns (Figure S1) of the Cu/ZrO_2 catalyst used in our experiments showed the presence of the cubic phase of ZrO_2. We chose the (111) surface as it was one of the stable surfaces of zirconia [41]. To accommodate the copper cluster with small lateral interactions between periodic images, the surface unit cell was increased to (3×3) super cell (see Figure 1(a)). The slab of metal oxide was chosen to contain two ZrO_2 molecules thick, thus six atomic layers in total. Previous studies showed that a model with six layers was sufficient to represent the geometric relaxation of zirconia surfaces [42]. The super cell had dimensions a=b=10.75 Å and c=19.4 Å, which included a vacuum region of thickness greater than 15 Å to ensure no interaction between the slabs. During the geometry optimizations of the bulk, the supercell was fully relaxed under the restriction of fixed cell parameters. We allowed the coordinates of two uppermost atomic layers of the slab, with their adsorbates to relax. The other and bottom atomic layers were held fixed at the bulk positions of the metal oxide.

The defect-free flat MgO (100) surface [43] was modeled by a $(2\sqrt{2} \times 3\sqrt{2})$ unit cell with three layers thick and 35 atoms per layer per supercell (see Figure 1(b)). Previous studies have shown that slabs of 3–4 layers provided a very good representation of the MgO (100) surface [44, 45]. A vacuum of at least 15 Å prevented the interaction between successive slabs. The lowest two layers were held frozen at the optimal DFT lattice constant of 4.21 Å, which was comparable to the experimental lattice constant (4.26 Å).

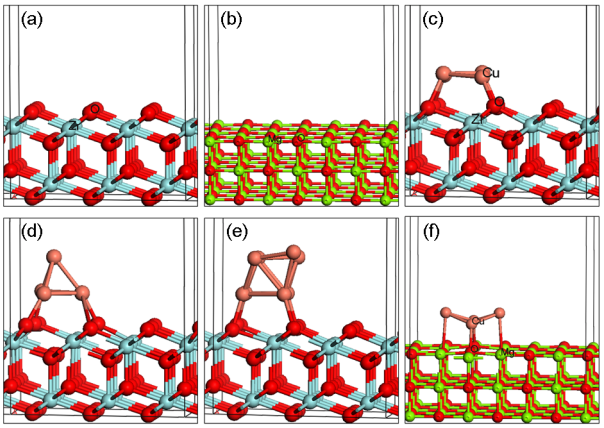

Figure 1 Side views of the optimized (a) (3×3) unit cell of ZrO_2 (111) surface. (b) $(2\sqrt{2} \times 3\sqrt{2})$ unit cell of MgO (100) surface. (c) Cu_4 supported on the ZrO_2 (111) surface in rhombic structure. (d) Cu_4 supported on the ZrO_2 (111) surface in tetrahedral structure. (e) Cu_8 cluster supported on the ZrO_2 (111) surface. (f) Cu_4 supported on the MgO (100) surface in a butterfly shape.

In this work, we calculated adsorption energies according to the following equation:

$$E_{ads}=E(\text{surface + adsorbate}) - E(\text{surface}) - E(\text{adsorbate}) \quad (1)$$

where E(surface + adsorbate), E(surface), and E(adsorbate) denote the calculated electronic energies of final optimized adsorption configurations, the bare surface, and a free molecule, respectively. With this definition, a negative E_{ads} value implied that the adsorption of molecules was thermodynamically favorable.

2.3 Experimental section

Two catalysts with a copper loading amount of 15 wt% were prepared, which were identified as Cu-15/MgO and Cu-15/ZrO_2. Accordingly, the Cu/Zr and Cu/Mg molar ratios equal 0.29 and 0.10, respectively. In our calculations, Cu_4/ZrO_2 (111)-(3×3) and Cu_4/MgO (100)-$(2\sqrt{2} \times 3\sqrt{2})$ models were used. The Cu/Zr and Cu/Mg molar ratios were calculated to be 0.22 and 0.11, respectively. From the above analysis, it can be found that the Cu/Zr and Cu/Mg ratios match well in our calculations and experiments. The detailed procedures of the catalyst preparation and characterization were given in the Supporting Information. The XRD patterns of the Cu/ZrO_2 catalyst (Figure S1) showed a number of peaks corresponding to 2θ = 30.5, 35.2, 50.7 and 60.5, which shows the presence of both *P4₂/nmc* tetragonal and *Fm3m* cubic phases. It is reported that most of the XRD peaks of the tetragonal and cubic phase of zirconia are

overlapped and it is very difficult to distinguish between the two from XRD patterns [46]. In the test of glycerol hydrogenolysis activity, the reaction was carried out in a batch system using a 100 mL stainless-steel autoclave (Weihai Bay Company). After 1 g catalyst and 50 mL 10 wt% aqueous glycerol solution were loaded, the reactor was purged four times with hydrogen to remove air and then pressured to 6.0 MPa, programmed to 453 K for a given period at a stirring speed of 800 rpm. After reaction, the reactor was cooled to room temperature; samples were filtered through 0.22-μm-pore-size filters (Membrana) to remove the solid catalyst powder prior to analysis and analyzed using a gas chromatograph (Varian 450-GC) equipped with a flame ionization detector (FID) and Galaxy workstation. The samples were injected (split ratio: 20) into a DB-FFAP column of 30 m × 0.32 mm and 0.25 μm phase thickness. The temperature program was from 60 °C (2 min) to 250 °C (8 min) at a rate of 20 °C/min. Injector and detector temperatures were 250 °C and 280 °C, respectively. The carrier gas used was N_2 at 1 mL/min. The FID used hydrogen at 30 mL/min. The makeup gas was N_2 at 29 mL/min.

3 Results and discussion

3.1 The surfaces of Cu/ZrO_2 (111)-(3×3) and Cu/MgO (100)-($2\sqrt{2} \times 3\sqrt{2}$)

Four copper atoms are used to mimic the smallest cluster-like construction of Cu-cluster on these two surfaces. Two possible Cu doping structures with different arrangement, a planar rhombic structure (Cu_4-p), and tetrahedral structure (Cu_4-t) are calculated, and the structures that exhibited the largest adsorption energies are obtained. The side views of the supported Cu4 clusters are plotted in Figure 1. It is worth mentioning that the ZrO_2 (111)-(3×3) and MgO (100)-($2\sqrt{2} \times 3\sqrt{2}$) super cells are sufficiently large to accommodate Cu_4 atoms.

The most stable arrangement of Cu_4 cluster on ZrO_2 (111) surface is in a rhombus structure (Figure 1(c)), as in the case of the free Cu_4 cluster [47]. Four Cu–O bonds are formed upon adsorption, with an average length of 1.99 Å. In addition, three Cu–Zr bonds are formed with an average long distance of 2.88 Å. This value is close to that found in previous theoretical investigation of the adsorption of a Cu atom on ZrO_2 showing a Cu–Zr distance of 2.74 Å. This reveals that the metal-metal interaction in the metal clusters decreases the metal-ZrO_2 (111) interaction [42]. The binding energy is calculated to be –45.8 kcal/mol. For the metastable tetrahedral structure (Figure 1(d)), the cluster-surface bonding scheme is different, with three Cu–O bonds (1.91 Å) and two Cu-Zr bonds (2.94 Å). The adsorption energy is estimated to be –36.9 kcal/mol.

The adsorbed Cu tetramer aggregated on MgO (100) surface has been previously investigated using density functional calculations. It was found that the most stable geometry for Cu_4 was a rhombus [48]. Consequently, we select the Cu_4 rhombus to explore its interaction with the supporting MgO (100) and the optimized structure is given in Figure 1(f). Upon relaxation, the adsorbed rhombus is shown not to be perfectly planar, which distorts with a butterfly shape. The Cu atoms at the end of the short diagonal attract their supporting oxygen by 2.12 and 2.13 Å, while the other two Cu atoms, staying further away on top of their oxygen, separated by distances of 2.91 and 2.92Å. The binding energy is found to be –26.0 kcal/mol.

A typical isomer of Cu_8 with D_{3d} symmetry in the gas phase has been considered to study copper octamer adsorption on ZrO_2 (111)-(3×3) surface. The optimized structure is presented in Figure 1(e). The average Cu–O distance in the bottom Cu_4 layer is found to be 1.98 Å, and the adsorption energy is predicted at –51.7 kcal/mol, which is comparable to the adsorption energy for Cu_4 cluster on the surface.

3.2 Hydrogenolysis of glycerol on the Cu/ZrO_2 (111) surface: DFT studies

The first step for glycerol hydrogenolysis reaction on the Cu/ZrO_2 (111) surface is the molecular chemisorption of glycerol and dissociative chemisorption of hydrogen. The metal-oxide interface has been proposed as a unique reaction site where reactants are activated, and it is known to be highly active for many heterogeneous catalytic reactions. We began the construction of the glycerol adsorbate in different orientations by adding the glycerol molecule onto the Cu_4/ZrO_2 (111) interface [49]. The energetically most favorable adsorption mode is depicted schematically in Figure 2(a), with the corresponding adsorption energy of –39.9 kcal/mol. In this case, the glycerol molecule is anchored on the top site of Cu cluster through one of the oxygen atoms in the terminal hydroxyl group. The distance between Cu and O is 2.18 Å. In addition, the oxygen atom in the sec-

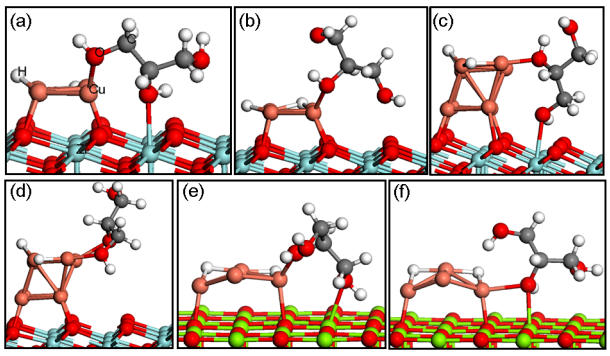

Figure 2 The optimized structures of glycerol and H_2 chemisorbed on the Cu_4/ZrO_2 (111) (a, b), Cu_8/ZrO_2 (111) (c, d), and Cu_4/MgO (100) (e, f) surfaces. The bottom part of the surface has been omitted, which is similar to the one shown in Figure 1.

ondary hydroxyl group interacts with a surface Zr site, with a Zr–O bond length of 2.49 Å. As previously suggested in the literature [23], the breaking H atoms of hydrogen sit above the Cu–Cu bridge site. The second most stable structure resulting from glycerol adsorption is shown in Figure 2(b), which binds slightly weakly to the surface with adsorption energy of −38.9 kcal/mol. It can be seen that the oxygen atom in the middle hydroxyl group adsorbs at the top of the Cu site. The Cu–O bond is calculated at 2.09 Å.

The adsorption structures of glycerol and H_2 on the Cu_8/ZrO_2 (111) catalyst are shown in Figures 2(c) and 2(d). The strongest binding mode has adsorption energy of −40.7 kcal/mol. The oxygen atom connected to the secondary C binds to a Cu atom. The Cu–O bond length is 1.96 Å. The oxygen atom attached to the primary carbon occupies on the top site of Zr. The Zr–O bond length is 2.58 Å. This hydroxyl group also points toward a lattice O atom that shows a hydrogen bonding of 1.76 Å. The second strongest binding structure has adsorption energy of −36.9 kcal/mol, where oxygen atoms from both primary and central hydroxyl groups adsorb on the Cu atoms. The Cu–O bond lengths are calculated to be 2.01 and 2.23 Å. Overall, no significant changes in total adsorption energies are found for glycerol interacting with Cu_4/ZrO_2 and Cu_8/ZrO_2 surfaces, suggesting that the smaller Cu_4 cluster is effective for probing the reactivity of bifunctional catalyst in the hydrogenolysis reaction.

An overview of the major thermochemical results is given in this section. On the basis of the above optimized adsorption configurations, the reaction mechanisms of glycerol over the Cu_4/ZrO_2 and Cu_8/ZrO_2 models to produce 1,2-PDO and 1,3-PDO are investigated. The structures for the most favorable configurations of intermediates are depicted in Figures 3 and 4, and the potential energy profiles of these routes are displayed in Figure 5.

The first step leading to 1,2-PDO product is the coadsorption of glycerol and H_2 at the interface of Cu_4/ZrO_2 forming 2(b), where the secondary hydroxyl coordinates to Cu. Next, a primary hydroxyl group in 2(b) is dehydrated via scissions of terminal C–OH bond and central C–H bond, to form the adsorbed propene-2,3-enol intermediate and water (Figure 3(a)).

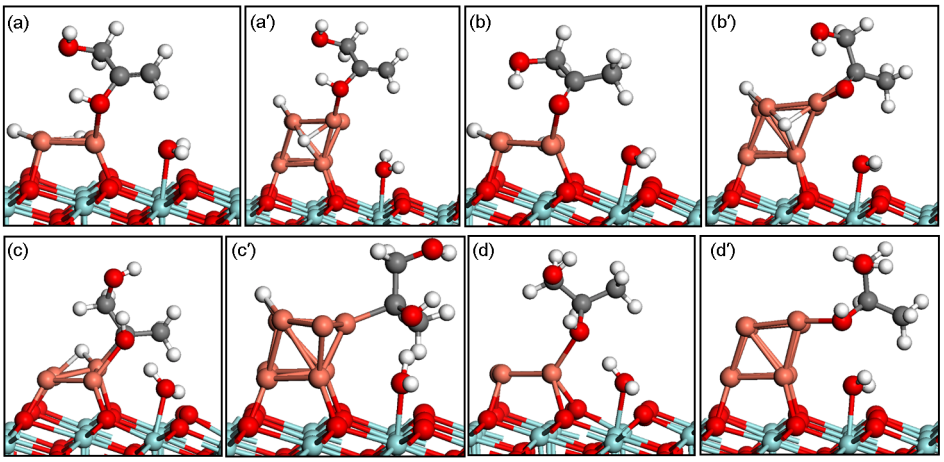

Figure 3 Structures of the intermediates for glycerol hydrogenolysis to 1, 2-PDO on the Cu_4/ZrO_2 (111) and Cu_8/ZrO_2 (111) surfaces.

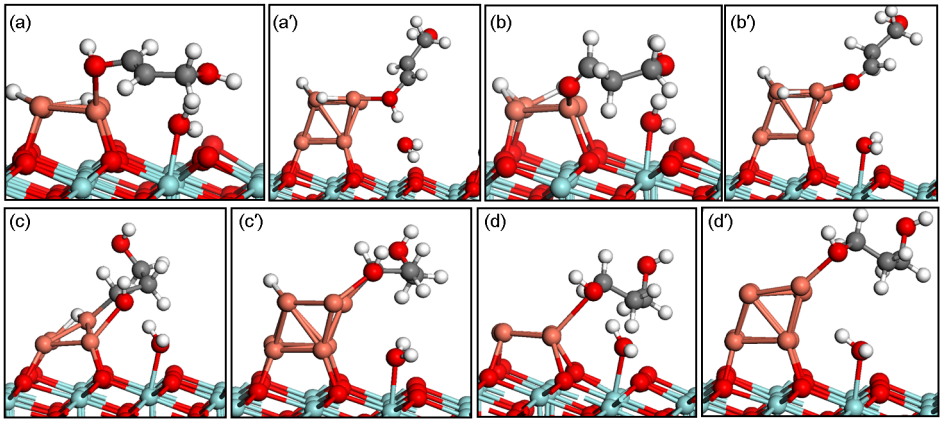

Figure 4 Structures of the intermediates for glycerol hydrogenolysis to 1, 3-PDO on the Cu_4/ZrO_2 (111) and Cu_8/ZrO_2 (111) surfaces.

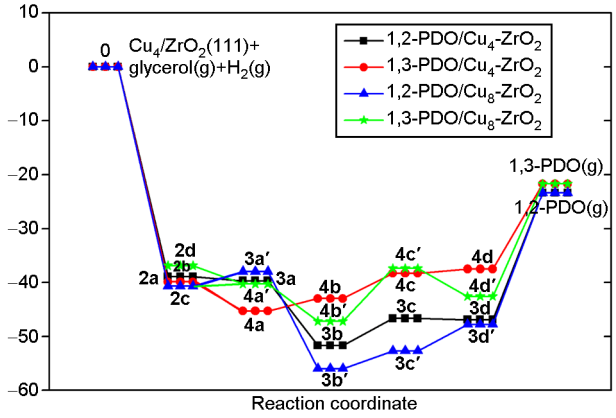

Figure 5 Reaction profiles for the glycerol hydrogenolysis on Cu_4/ZrO_2 (111) and Cu_8/ZrO_2 (111). The zero energy is taken as the sum of the energies of Cu_4/ZrO_2 (111), the gas-phase glycerol, and gas phase hydrogen. The black line represents the formation of 1,2-PDO, and the red line represents the formation of 1,3-PDO. The formations of 1,2-PDO and 1,3-PDO on a larger Cu_8 cluster are also given and represented by the blue and green lines.

The 2, 3-enol species is bound to a Cu atom through the oxygen atom in the secondary hydroxyl group (O–Cu bond equals 2.26 Å). The releasing water molecule occupies on the top site of a lattice Zr with O–Zr length of 2.37 Å. This step is slightly exothermic by 0.8 kcal/mol. The 2,3-enol species can be rearranged further in acetol intermediate (Figure 3(b)), corresponding to the migration of H atom from central OH group in 3(a) to the CH_3 fragment in 3(b). The adsorbed acetol species is featured by the keto oxygen binding to a Cu atom with a Cu–O bond length of 2.13 Å. The reaction energy of this step is calculated to be –12.0 kcal/mol. In the third step, a hydrogen atom adsorbed across the Cu2 bridge site can combine with the keto oxygen in 3(b) to produce a semi-hydrogenated intermediate (Figure 3(c)). This species forms a ring structure attached on the Cu cluster via its central O atom and undercoordinated C atom. The C–Cu and O–Cu bond lengths are 1.99 Å and 2.15 Å. In addition, this partially hydrogenated species 3(c) is stabilized by a weak hydrogen bonding formed between its oxygen atom connected to central carbon and the O–H group in water at a distance of 1.73 Å. The reaction energy for the conversion is 5.0 kcal/mol. The last step converts 3(c) to the adsorbed 1,2-PDO species (Figure 3(d)) by transferring another chemisorbed H atom to the undercoordinated carbon in 3(c). The oxygen atom bonded to the secondary carbon binds to a Cu atom forming a Cu–O bond of 2.25 Å. As shown in Figure 5, this step is slightly exothermic by –0.2 kcal/mol.

The initial step on the pathway leading to 1,3-PDO production concerns the decomposition of glycerol in 2(a) into the propene-1,3-enol intermediate through breaking of the central C–OH bond and terminal C–H bond (Figure 4(a)). The oxygen atom connected to the primary carbon binds to the top site of Cu. The Cu–O bond length is 2.27 Å. The oxygen atom of released water attaches to a Zr atom with O–Zr bond length of 2.25 Å. This step is exothermic by –5.4 kcal/mol. The second step proceeds through the isomerization of 1,3-enol intermediate into the adsorbed 3-hydroxypropanal species with a reaction heat of 2.3 kcal/mol. A shift of one H occurs from the terminal hydroxyl group in 4(a) to the central carbon group in 4(b), involving the coordination of the carbonyl O on the Cu cluster that shows a Cu–O distance of 2.03 Å (Figure 4(b)). In the third step, one hydrogen atom begins to move away from the bridge site of Cu_2 and jumps to the oxygen atom in the aldehyde group, resulting in the formation of a semi-hydrogenated species (Figure 4(c)). The C–Cu and O–Cu distances are 1.97 and 2.30 Å, respectively. This step exhibits a reaction heat of 4.7 kcal/mol. At the final step, another H atom can attack the unsaturated carbon in 4(c) to obtain the 1,3-PDO, which is endothermic by –0.8 kcal/mol. The oxygen of primary hydroxyl group is located above the Cu atom with Cu–O distance of 2.17 Å (Figure 4(d)).

On Cu_8/ZrO_2, the propene-2,3-enol species (3(a′)) resulting from primary C–O bond and secondary C–H bond scissions in 2(c) resembles that on the Cu_4/ZrO_2 surface. The hydroxyl group attached to the middle C binds to the Cu_8 cluster. The Cu–O distance is 2.10 Å. The detached water molecule points towards the surface Zr site at a distance of 2.37 Å. Our calculated reaction heat of this step is 2.7 kcal/mol. In the second step, the acetol intermediate 3(b′) is formed and binds to the Cu_8 cluster via both carbon and oxygen atoms in the carbonyl group. The Cu–O and Cu–C distances are 1.96 and 2.15 Å. The bidentate coordination implies a strong interaction, which is verified by the calculated reaction heat of –18.0 kcal/mol. In the following step of transferring one dissociated H atom to the carbonyl oxygen in 3(b′) to form a semi-hydrogenated species 3(c′), a different structure is obtained. The hydroxyl group attached to the middle carbon no longer adsorbs at the top site of Cu atom. Instead, it prefers to point at the terminal hydroxyl group of water bound to ZrO_2 surface, forming a hydrogen bond-like structure at a O···H length of 1.56 Å. Besides, we found the central carbon atom binds to a top site of Cu_8 cluster with a Cu–C distance of 1.97 Å. The computed reaction heat of this step is 3.3 kcal/mol. The Cu–C bond is dissociated when the second hydrogen atom moves towards the unsaturated carbon in 3(c′) and the secondary hydroxyl group approaches the top site of Cu8 cluster, yielding an adsorbed 1,2-PDO species 3(d′). It was found to be analogous to 1,2-PDO adsorbed on the Cu_4 cluster. Our calculations give a positive reaction energy of 4.9 kcal/mol associated with this process.

As depicted in Figure 4, the propene-1,3-enol species 4(a′) resulting from glycerol decomposition of 2(d) is preferentially adsorbed on the top site of the Cu_8 cluster via its terminal hydroxyl group with a Cu–O distance of 1.96 Å. Simultaneously, the hydroxyl H atom also closely interacts

with the water O atom with a O··H distance of 1.62 Å. The strong hydrogen bond results in a long distance between the water molecule and surface Zr site (2.62 Å). This step is slightly exothermic by 3.4 kcal/mol. The subsequent 3-hydroxypropanal structure 4(b′) is similar to that on the Cu4 cluster, where the aldehyde oxygen atom occupies the top site of Cu with a Cu–O distance of 1.92Å. The calculations indicate a moderate reaction heat of –6.9 kcal/mol. The semi-hydrogenated species 4(c′) binds strongly to the Cu8 cluster. The preferred binding mode seems to be a four-membered ring with the C–O bond parallel to the Cu–Cu bond. The Cu–C and Cu–O distances are 1.97 and 2.11 Å, respectively. Different from the intermediate on the Cu4 cluster, the water H atom points away from the terminal hydroxyl O atom. This step proceeds with a positive reaction heat of 9.8 kcal/mol. The migration of the hydrogen atom from Cu_2 bridge site to the terminal C atom in 4(c′) yielding an adsorbed 1,3-PDO 4(d′), is a modest exothermic process (–5.2 kcal/mol), with the primary hydroxyl oxygen anchored to the Cu atom at a distance of 2.11 Å.

As illustrated in Figure 5, we found that the formation of 1,2-PDO is much easier than 1,3-PDO on the Cu cluster from the thermodynamic viewpoint, which can be proved by the much lower energies of the adsorbed intermediates at each stage of glycerol hydrogenolysis to produce 1,2-PDO (except for the first step regarding enols formation). The reaction energies differ significantly along the 1,2-PDO and 1,3-PDO pathways with the value reaching as large as 8.4 kcal/mol on Cu4 cluster and 15.3 kcal/mol on Cu8 cluster, suggesting that this surface will be selective to 1,2-PDO. Vasiliu *et al*. presented a detailed computational study of the thermodynamic properties for the conversion of glycerol into propanediols in the gas, liquid and water solutions [50]. The calculated values for the Gibbs free energies showed that the formations of 1,2-PDO and 1,3-PDO were highly exothermic processes, with a feasible formation of 1,2-PDO. These results were consistent with the reactions performed using the Cu-based catalysts.

3.3 Hydrogenolysis of glycerol on the Cu_4/MgO (100) surface: DFT studies

The adsorption structures of glycerol and H_2 on the Cu_4/MgO (100) interface are illustrated in Figures 2(e) and 2(f). The glycerol molecule can adsorb through a bi-dentate anchoring geometry (2(e)): its central oxygen atom prefers the top site of Cu, and the terminal oxygen favors the top site of lattice Mg, with the newly formed Cu–O and Mg–O bonds being about 2.09 and 2.40 Å. The adsorption is exothermic by –49.1 kcal/mol. The optimal structure of glycerol and hydrogen chemisorbed on Cu/MgO is given in Figure 2(f). Different from 2(e) with secondary hydroxyl coordinated to Cu and primary hydroxyl to Mg, the Cu cluster and the surface Mg site are capable of simultaneously interacting with the secondary hydroxyl group. The Cu–O and Mg–O distances are 2.26 and 2.33 Å. The calculated adsorption energy is –59.3 kcal/mol.

The optimal structure 2(f) is chosen as the initial geometry for the hydrolysis of glycerol on Cu_4/MgO. The primary hydroxyl is dehydrated leading to 1,2-PDO and a secondary hydroxyl is dehydrated leading to 1,3-PDO. The proposed pathways are schematically depicted in Figures 6 and 7, and the calculated corresponding potential-energy surfaces are drawn in Figure 8.

In an analogous way, glycerol dissociation initially occurs via successive rupture of terminal C–O bond and central C–H bond to yield 2,3-enol intermediate (Figure 6(a)). The detached water molecule would preferably adsorb onto the Cu atom and Mg atom of the MgO surface. This step is endothermic by 9.3 kcal/mol. Then this 2,3-enol species converts into an acetol intermediate, which is constructed by the carbonyl oxygen atom interacting simultaneously with a Cu atom and lattice Mg (Figure 6(b)). The Cu–O and Mg–O distances correspond to 2.11 and 2.62 Å, respectively.

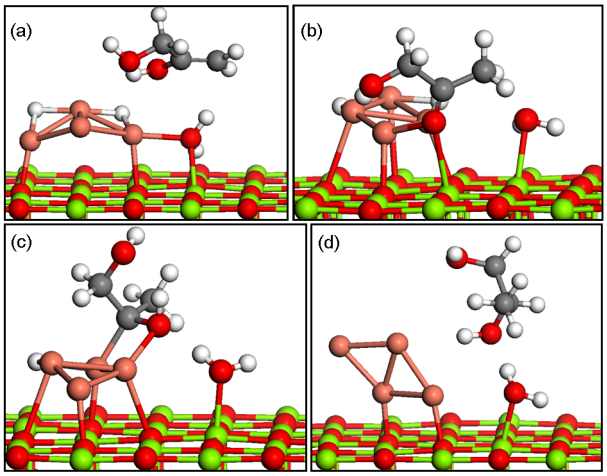

Figure 6 Structures of the intermediates for glycerol hydrogenolysis to 1,2-PDO on the Cu_4/MgO (100) surface.

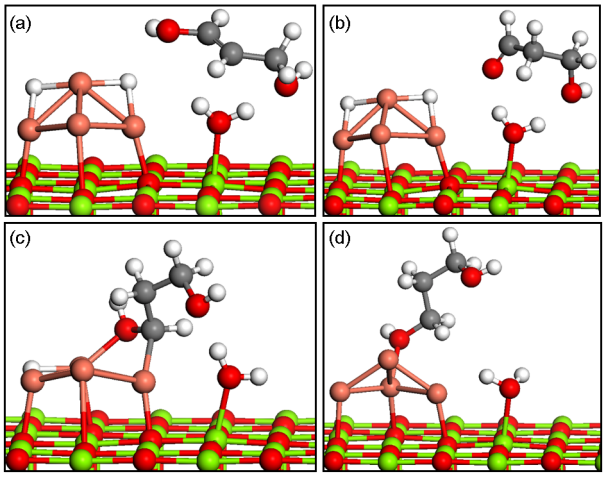

Figure 7 Structures of the intermediates for glycerol hydrogenolysis to 1,3-PDO on the Cu_4/MgO (100) surface.

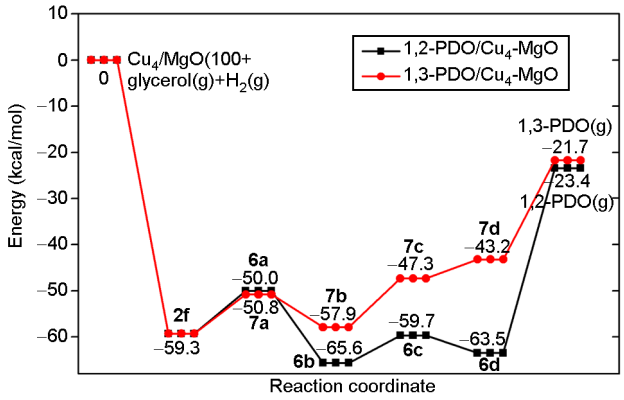

Figure 8 Reaction profiles for the glycerol hydrogenolysis on Cu_4/MgO (100). The zero energy is taken as the sum of the energies of Cu_4/MgO (100), the gas-phase glycerol, and gas phase hydrogen. The black line represents the formation of 1,2-PDO, and the red line represents the formation of 1,3-PDO.

The calculated reaction energy is −15.6 kcal/mol. Subsequently, one hydrogen atom formed by dissociation adsorption migrates to the carbonyl oxygen end of the acetol intermediate and results in a semi-hydrogenated species characterized by a four-membered-ring structure (Figure 6(c)). The C–Cu and O–Cu bonds are predicted at 1.97 and 2.02 Å, which requires a reaction energy of 5.9 kcal/mol. Further hydrogenation at the unsaturated C end in 6(c) with another isolated hydrogen atom produces the 1,2-PDO (Figure 6(d)). In this step, the central oxygen atom is attracted by the adjacent H atom in water generating a weak hydrogen bonding (O···H=1.86 Å). The reaction is exothermic by 3.8 kcal/mol.

Next, we turn to the reaction route for the formation of 1,3-PDO on the Cu_4/MgO model system. The first formation of 1,3-enol intermediate takes places via the decomposition of glycerol through cleavage of central C–OH group and terminal C–H bond (Figure 7(a)). The 1, 3-enol species interacts with the eliminated water molecule via a hydrogen bonding coordination (1.73 Å). This step is endothermic by 8.5 kcal/mol. Once the 1,3-enol intermediate is formed it can easily convert into the 3-hydroxypropanal intermediate (Figure 7(b)). During this reaction, two kinds of hydrogen bonding are identified. The former is formed by the oxygen end of C=O bond incorporating with a hydrogen atom from detached water; the latter is formed by the oxygen bonded to the primary C pointing to the other H in water. The O···H bonds are computed to be 1.86 and 1.99 Å, respectively. This transformation reaction is exothermic by 7.1 kcal/mol. This is followed by the addition of a H atom located at Cu_2 site to the hydroxypropanal intermediate at the carboxyl O end (Figure 7(c)), forming one Cu–C bond (1.95 Å) and one Cu–O bond (2.01 Å). The reaction energy of this step is 10.6 kcal/mol. The last step involves the coupling of the second H with the unsaturated C end in **7(c)** to yield the 1,3-PDO (Figure 7(d)). The oxygen in the terminal hydroxyl group is brought close to the Cu cluster and a new Cu–O bond is created with a length of 2.16 Å. This step is calculated to be endothermic by 4.1 kcal/mol. In summary, although the 1,2-PDO and 1,3-PDO reaction pathways via the hydrogenolysis of glycerol are facile on the Cu/MgO surface from thermodynamics (Figure 8), the results clearly demonstrate the relative stability of the intermediates on each stage of 1,2-PDO formation are much higher than that of the corresponding 1,3-PDO (except for the first step). The energy difference reaches 20.3 kcal/mol on Cu_4/MgO. Hence, 1,2-PDO is the thermodynamically preferred products. The finding is in line with the results predicted on the Cu_4/ZrO_2 surface.

3.4 The effect of support on the hydrogenolysis reaction: Comparisons with experiments

The results mentioned above apparently indicate that the support plays a role in determining the unique catalytic activities of Cu clusters. The MgO substrate shows superior activities than ZrO_2 in the production of 1,2-PDO (Figures 5 and 8). The acid-base characteristic of Mg and O sites on MgO enhances the interaction between glycerol and the Cu/MgO catalyst. A similar behavior has been reported in the literature for the interaction of glycerol with flat MgO (001) [51]. In addition, the MgO surface has greater affinity toward water [52] than ZrO_2, thus favors the dehydration of glycerol to hydroxyacetone, which may have a positive effect on the catalytic activity. Our results indicate that for propanediol production from glycerol hydrogenolysis, catalysts with high initial-step dehydration activity should be developed.

The experimental results of conversions and selectivities of glycerol catalyzed by Cu/ZrO_2 and Cu/MgO catalysts are presented in Figure 9. The results show that both catalysts exhibit high catalytic activity in the hydrogenolysis of glycerol. 1,2-PDO and ethylene glycol are detected as the main products under our present experimental conditions. This is in agreement with the thermodynamic profiles of this reaction predicted from first-principles simulation that shows the Cu catalysts give the 1,2-PDO as a dominant product. Furthermore, the formation of 1,2-PDO is largely promoted by employing the Cu/MgO catalyst in contrast to Cu/ZrO_2. When Cu/MgO is used as a catalyst, the conversion of glycerol increases from 52.2% to 85.2% with increasing the time from 8 h to 40 h. However, the selectivity of 1,2-PDO decreases from 95.1% to 90.9%. When the hydrogenolysis reaction is catalyzed by Cu/ZrO_2, the conversion of glycerol increases gradually from 43.2% to 81.9% with the increase of time from 8 h to 40 h. The selectivity of 1,2-PDO reduces from 87.6% to 85% accordingly. The experimentally observed reactivity trend is in line with our calculated result demonstrating that Cu/MgO exhibits superior activities than Cu/ZrO_2 in the yield of 1,2-PDO from the thermodynamic viewpoint.

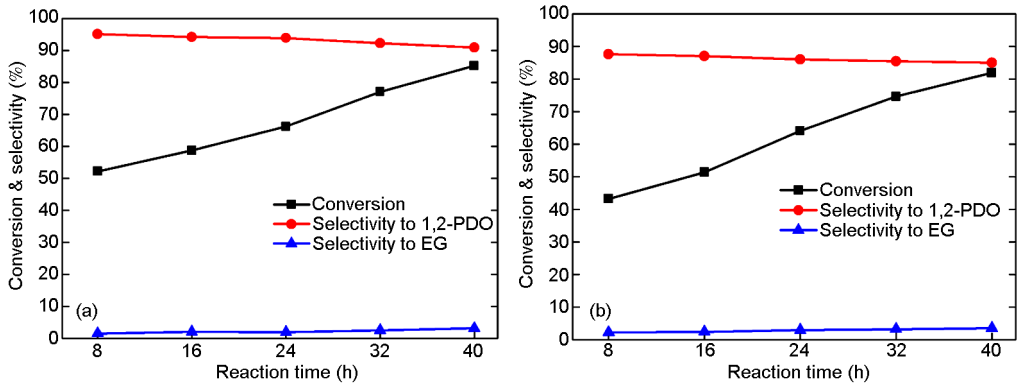

Figure 9 Time course of glycerol hydrogenolysis to 1,2-PDO over Cu/MgO (a) and Cu/ZrO_2 (b). Reaction conditions: 50.0 mL of 10 wt.% aqueous solution of glycerol, 1.0 g of reduced catalyst, H_2 pressure 6.0 MPa.

It is important to emphasize that our analysis of the 1,2-PDO/1,3-PDO selectivity is based only on the adsorption thermochemistry of glycerol dehydrated and hydrogenated intermediates. An explicit kinetic analysis, involving the most stable transition states at each level of the pathway, would provide a more precise prediction of the selectivity patterns of glycerol hydrogenolysis over Cu-based catalysts than the thermochemistry analysis that we have presented above. The activation energy is the key parameter that controls the overall rate and the selectivity. It has been reported that the elimination of a secondary alcohol proceeds via a relatively stable secondary carbocation and is therefore kinetically controlled. The elimination of a primary alcohol forms acetol, which is thermodynamically more stable compared with 3-hydroxypropanal [53]. This consideration is the basis for higher 1,2-PDO selectivity than 1,3-PDO in most examples. We think that the kinetic analysis would be unlikely to change the important conclusions of this work, which demonstrates that 1,2-PDO production is favored. However, the selectivity of 1,3-PDO in the hydrogenolysis can be improved by altering transition energies, by developing the appropriated catalytic system, which will be explained in the framework of our future study.

4 Conclusions

The thermodynamic profiles for the hydrogenolysis of glycerol over bifunctional copper-based catalysts, Cu/ZrO_2 and Cu/MgO, to produce propanediols have been calculated using the first-principles calculations. The hydrogenolysis productivity and selectivity to yield 1,2-PDO and 1,3-PDO were compared. The reaction is started by glycerol dehydration leading to propene-2,3-enol and propene-1,3-enol intermediates. This step can be realized on the metal oxide surface by the acid-base catalysis. This is followed by isomerizations of these produced species into acetol or 3-hydroxypropanal. The final step is hydrogenation toward propanediols through successive migrations of H atoms to the C=O bond which requires the metal centers.

It has been demonstrated that the supported Cu cluster consisting of four Cu atoms as catalysts is sufficient to describe the adsorption properties of glycerol in the reaction process. The results of reaction energetics show that the propanediols synthesis is fairly feasible on both catalysts. The modified stability of intermediates may have great influence on the 1,2-PDO and 1,3-PDO selectivity of the reaction. This might explain why only 1,2-PDO is obtained on the Cu-based catalysts. In addition, the relative stability of these intermediates is strongly dependent on the choice of metal oxide support. This may exert great influence on the activity of the reaction. From a global thermodynamic viewpoint, Cu/MgO is much more effective than Cu/ZrO_2 in the hydrogenolysis of glycerol molecule. The experimentally observed activity and selectivity trends are consistent with the DFT calculations. The fundamental understanding of the structural, energetics, and catalytic properties of Cu-based catalysts for glycerol hydrogenolysis investigations in this work may improve our ability to tune catalysts for increased activity and selectivity.

We acknowledge the financial support from the Natural Science Foundation of Shandong Province (ZR2010BQ001 and O92003110C) and the National Natural Science Foundation of China (20803038).

1 Werpy T, Petersen G. Top value added chemicals from biomass, vol. 1–Results of screening for potential candidates from sugars and synthesis gas. *US DOE Report*, 2004
2 Chiu C, Dasari M, Sutterlin W, Suppes G. Removal of residual catalyst from simulated biodiesel's crude glycerol for glycerol hydrogenolysis to propylene glycol. *Ind Eng Chem Res*, 2006, 45: 791–795
3 Chaminand J, Djakovitch L, Gallezot P, Marion P, Pinel C, Rosierb C. Glycerol hydrogenolysis on heterogeneous catalysts. *Green Chem*, 2004, 6: 359–361
4 Akiyama M, Sato S, Takahashi R, Inui K, Yokota M. Dehydration-hydrogenation of glycerol into 1,2-propanediol at ambient hydrogen pressure. *Appl Catal A: Gen*, 2009, 371: 60–66
5 Dasaria M, Kiatsimkula P, Sutterlinb W, Suppes G. Low-pressure hydrogenolysis of glycerol to propylene glycol. *Appl Catal A: Gen*, 2005, 281: 225–231
6 Yuan Z, Wang J, Wang L, Xie W, Chen P, Hou Z, Zheng X. Biodiesel derived glycerol hydrogenolysis to 1,2-propanediol on

Cu/MgO catalysts. *Biores Technol*, 2010, 101: 7088–7092
7 Perosa A, Tundo P. Selective hydrogenolysis of glycerol with raney nickel. *Ind Eng Chem Res*, 2005, 44: 8535–8537
8 Furikado I, Miyazawa T, Koso S, Shimao A, Kunimori K, Tomishige K. Catalytic performance of Rh/SiO_2 in glycerol reaction under hydrogen. *Green Chem*, 2007, 9: 582–588
9 Maris EP, Davis RJ. Hydrogenolysis of glycerol over carbon-supported Ru and Pt catalysts. *J Catal*, 2007, 249: 328–337
10 Miyazawa T, Kusunoki Y, Kunimori K, Tomishige K. Glycerol conversion in the aqueous solution under hydrogen over Ru/C + an ion-exchange resin and its reaction mechanism. *J Catal*, 2006, 240: 213–221
11 Runberg A, Baiker J, Kijenski J. Copper catalyzed amination of ethylene glycol. *Appl Catal*, 1985, 17: 309–319
12 Vasiliadou ES, Heraclous E, VasalosI A, Lemondiou AA. Ru-based catalysts for glycerol hydrogenolysis–Effect of support and metal precursor. *Appl Catal B: Environ*, 2009, 92: 90–99
13 Yuan ZL, Wu P, Gao J, Lu XY, Hou ZY, Zheng XM. Pt/solid-base: A predominant catalyst for glycerol hydrogenolysis in a base-free aqueous solution. *Catal Lett*, 2009, 130: 261–265
14 Wang S, Liu H. Selective hydrogenolysis of glycerol to propylene glycol on Cu-ZnO catalysts. *Catal Lett*, 2007, 117: 62–67
15 Cameron DC, Cooney CL. A novel fermentation: The production of R(-)-1,2-propanediol and acetol by Clostridium thermosaccharolyticum. *Biotechnol*, 1986, 4: 651–654
16 Cameron DC, Altaras NE, Hoffman ML, Shaw AJ. Metabolic engineering of propanediol pathways. *Biotechol Prog*, 1998, 14: 116–225
17 Montassier C, Giraud D, Barbier J. Polyol conversion by liquid phase heterogeneous catalysis over metals. *Heter Catal Fine Chem*, 1988, 41: 165–170
18 Montassier C, Menezo JC, Hoang LC, Renaud C, Barbier J. Aqueous polyol conversions on ruthenium and on sulfur-modified ruthenium. *J Mol Catal*, 1991, 70: 99–110
19 Zheng AM, Chen L, Yang J, Zhang MJ, Su YC, Yue Y, Ye CH, Deng F. Combined DFT theoretical calculation and solid-state NMR studies of Al substitution and acid sites in zeolite MCM-22. *J Phys Chem B*, 2005, 109: 24273–24279
20 Yang G, Zhou LJ, Liu XC, Han XW, Bao XH. H_2 adsorption on Fe/ZSM-5 zeolite: A theoretical approach. *J Phys Chem B*, 2006, 110: 22295–22297
21 Zheng AM, Zhang HL, Lu X, Liu SB, Deng F. Theoretical predictions of ^{31}P NMR chemical shift threshold of trimethylphosphine oxide absorbed on solid acid catalysts. *J Phys Chem B*, 2007, 112: 4496–4505
22 Yang G, Zhou LJ, Liu XC, Han XW, Bao XH. Reaction mechanisms of H_2 reduction and N_2O decomposition on Fe/ZSM-5 zeolite: A density functional theoretical study. *J Phys Chem C*, 2009, 113: 18184–18190
23 Chen Y, Salciccioli M, Vlachos DG. An efficient reaction pathway search method applied to the decomposition of glycerol on platinum. *J Phys Chem C*, 2011, 115: 18707–18720
24 Liu B, Greeley J. Decomposition pathways of glycerol via C–H, O–H, and C–C bond scission on Pt(111): A density functional theory study. *J Phys Chem C*, 2011, 115: 19702–19709
25 Michel C, Auneau F, Delbecq F, Sautet P. C–H versus O–H bond dissociation for alcohols on a Rh(111) surface: A strong assistance from hydrogen bonded neighbors. *ACS Catal*, 2011, 1: 1430–1440
26 Coll D, Delbecq F, Arayb Y, Sautet P. Stability of intermediates in the glycerol hydrogenolysis on transition metal catalysts from first principles. *Phys Chem Chem Phys*, 2011, 13: 1448–1456
27 Auneau F, Michel C, Delbecq F, Pinel C, Sautet P. Unravelling the mechanism of glycerol hydrogenolysis over rhodium catalyst through combined experimental-theoretical investigations. *Chem Eur J*, 2011, 17: 14288–14299
28 Kresse G, Furthmuller J. Efficient iterative schemes for ab initio total-energy calculations using a plane-wave basis set. *Phys Rev B*, 1996, 54: 11169–11186
29 Kresse G, Hafner J. Ab initio molecular-dynamics simulation of the liquid-metal-amorphous-semiconductor transition in germanium. *Phys Rev B*, 1994, 49: 14251–14269
30 Blochl PE. Projector augmented-wave method. *Phys Rev B*, 1994, 50: 17953–17979
31 Kresse G, Joubert D. From ultrasoft pseudopotentials to the projector augmented-wave method. *Phys Rev B*, 1999, 59: 1758–1775
32 Perdew JP, Wang Y. Accurate and simple analytic representation of the electron-gas correlation energy. *Phys Rev B*, 1992, 45: 13244–13249
33 Monkhorst HJ, Pack JD. Special points for Brillouin-zone integrations. *Phys Rev B*, 1976, 13: 5188–5192
34 Yang Z, Xie L, Ma D, Wang G. Origin of the high activity of the ceria-supported copper catalyst for H_2O dissociation. *J Phys Chem C*, 2011, 115: 6730–6740
35 Pan Y, Liu C, Ge Q. Effect of surface hydroxyls on selective CO_2 hydrogenation over Ni_4/c-Al_2O_3: A density functional theory study. *J Catal*, 2010, 272: 227–234
36 Valero MC, Raybaud P, Sautet P. Interplay between molecular adsorption and metal-support interaction for small supported metal clusters: CO and C_2H_4 adsorption on Pd_4/γ- Al_2O_3. *J Catal*, 2007, 247: 339–355
37 Chen HL, Peng WT, Ho JJ, Hsieh HM. Density-functional calculation of the adsorption and reaction of CO and H_2O molecules over a 4Rh/CeO_2(111) surface. *Chem Phys*, 2008, 348: 161–168
38 Zhang RG, Wang BJ, Liu HY, Ling LX. Effect of surface hydroxyls on CO_2 hydrogenation over Cu/γ-Al_2O_3 catalyst: A theoretical study. *J Phys Chem C*, 2011, 115: 19811–19818
39 Dongare MK, Malshe K, Gopinath CS, Murwani IK, Kemnitz E. Oxidation activity and ^{18}O-isotope exchange behavior of nickel oxide-stabilized cubic zirconia. *J Catal*, 2004, 222: 80–86
40 Meinel K, Eichler A, Schindler KM, Neddermeyer H. STM, LEED, and DFT characterization of epitaxial ZrO_2 films on Pt(1 1 1). *Surf Sci*, 2004, 562: 204–218
41 Gennard S, Cora F, Richard C, Catlow CRA. Comparison of the bulk and surface properties of ceria and zirconia by ab Initio investigations. *J Phys Chem B*, 1999, 103: 10158–10170
42 Grau-Crespo R, Hernández NC, Sanz JF, De Leeuw NH. Theoretical investigation of the deposition of Cu, Ag, and Au atoms on the ZrO_2(111) surface. *J Phys Chem C*, 2007, 111: 10448–10454
43 Tasker PW. The stability of ionic crystal surfaces. *J Phys C*, 1979, 12: 4977–4984
44 Mejías JA, Márquez AM, Fernández Sanz J, Fernández-García M, Ricart JM, Sousa C, Illas F. On modelling the interaction of CO on the MgO(100) surface. *Surf Sci*, 1995, 327: 59–73
45 Chen L, Wu R, Kioussis N, Zhang Q. First principles determinations of the bonding mechanism and adsorption energy for CO/MgO(001). *Surf Sci*, 1998, 290: 255–260
46 Joo J, Yu T, Kim YW, Park HM, Wu F, Zhang JZ, Hyeon TJ. Multigram scale synthesis and characterization of monodisperse tetragonal zirconia nanocrystals. *J Am Chem Soc*, 2003, 125: 6553–6557
47 Jug K, Zimmermann B, Calaminici P, Köster AM. Structure and stability of small copper clusters. *J Chem Phys*, 2002, 116: 4497–4507
48 Musolino V, Selloni A, Car R. First principles study of adsorbed Cu_n (n=1–4) microclusters on MgO(100): Structural and electronic properties. *J Chem Phys*, 1998, 108: 5044–5054
49 Rodriguez JA, Evans J, Graciani J, Park J, Liu P, Hrbek J, Sanz JF. High water-gas shift activity in TiO_2(110) supported Cu and Au nanoparticles: Role of the oxide and metal particle size. *J Phys Chem C*, 2009, 113: 7364–7370
50 Vasiliu M, Guynn K, Dixon DA. Prediction of the thermodynamic properties of key products and intermediates from biomass. *J Phys Chem C*, 2011, 115: 15686–15702
51 Calatayud M, Ruppert AM, Weckhuysen BM. Theoretical study on the role of surface basicity and Lewis acidity on the etherification of glycerol over alkaline earth metal oxides. *Chem Eur J*, 2009, 15: 10864–10870
52 Carrasco J, Illas F, Lopez N. Dynamic ion pairs in the adsorption of isolated water molecules on alkaline-earth oxide (001) surfaces. *Phys Rev Lett*, 2008, 100: 016101–016104
53 Nimlos MR, Blanksby SJ, Qian X, Himmel ME, Johnson DK. Mechanisms of glycerol dehydration. *J Phys Chem A*, 2006, 110: 6145–6156

SCIENCE CHINA
Chemistry

• SUPPORTING INFORMATION •

June 2013 Vol.56 No.6: 1–2
doi: 10.1007/s11426-012-4828-y

Thermodynamics of glycerol hydrogenolysis to propanediols over supported copper clusters: Insights from first-principles study

GUAN Jing, WANG XiCheng, WANG XiaoYan & MU XinDong*

Key Laboratory of Biofuels, Qingdao Institute of Bioenergy and Bioprocess Technology, Chinese Academy of Sciences, Qingdao 266101, China

Received October 25, 2012; accepted December 10, 2012; published online January 21, 2013

1 Catalyst preparation

1.1 Meterials

$Cu(NO_3)_2 \cdot 3H_2O$, AR, Sinopharm Chemical Reagent Co., Ltd, China; $Mg(NO_3)_2 \cdot 6H_2O$, AR, Shanghai Chemicals, China; $Zr(NO_3)_2 \cdot 2H_2O$, AR, Tianjin Guangfu Chemicals, China; Na_2CO_3, AR, Guangzhou Chemicals, China.

1.2 Method

The catalyst precursors were prepared by precipitation of a mixed aqueous solution of $Cu(NO_3)_2 \cdot 3H_2O$ and $Mg(NO_3)_2 \cdot 6H_2O$ (or $Zr(NO_3)_2 \cdot 2H_2O$, total metal concentration was 1 mol/L) by drop-wise adding of Na_2CO_3 solution (1 mol/L) under vigorous stirring at room temperature until the pH of the mixed solution reached 10.5 (Sartorius PB-10, Germany). After addition of the Na_2CO_3 solution, the resulting precipitates were aged under continuous stirring in the mother liquor at room temperature for 12 h. The suspensions were purged out of the reactor followed by separation of the precipitates from the mother liquor by vacuum filtration. After filtering, the resulting filter cake was washed thoroughly with deionized water. Finally, the washed precipitates were dried in ambient at 393 K for 12 h, followed by calcination at 823 K in static air for 4 h (5 K/min). Reduction of the catalysts were performed in pure H_2 atmosphere at 623 K at a heat ramp rate of 5 K/min, followed by an isothermal period of 1 h at the final temperature. Prior to exposure to air, the catalysts were passivated by purging reactor with 1% O_2/N_2 for 2 h at room temperature. Two catalysts with copper loading amount of 15 wt% were prepared in above procedures, which were identified as Cu-15/MgO and Cu-15/ZrO_2. The X-ray powder diffraction (XRD) patterns of catalysts were obtained with a Bruker D8 Advance X-ray diffractometer under Ni-filtered Cu-Kα radiation. Particle sizes of Cu were calculated from XRD patterns using Debye–Scherrer equation.

2 Characterization results

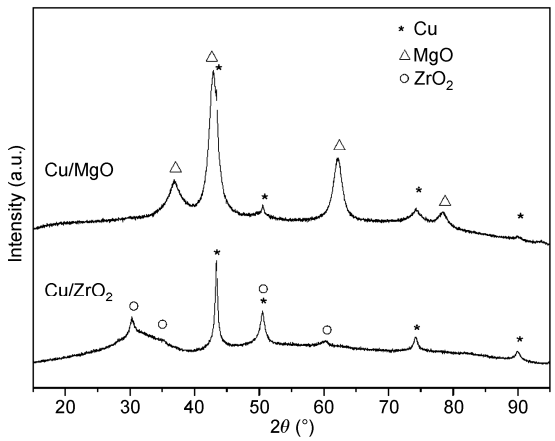

Figure S1 XRD patterns of Cu/MgO and Cu/ZrO_2 catalysts.

Table S1 Chemical properties of the Cu/MgO and Cu/ZrO_2 catalysts detected by XRD characterization

Catalyst	MgO/ZrO_2 crystallite size (nm)	Cu particle size (nm)	Metal loading (wt%)
Cu/MgO	13.9	21.0	~15%
Cu/ZrO_2	13.8	16.7	

*Corresponding author (email: muxd@qibebt.ac.cn)

Table S2 Glycerol hydrogenolysis over Cu/MgO and Cu/ZrO_2 catalysts[a)]

Catalyst	Reaction time (h)	Glycerol conversion (%)	Selectivity (%)		
			1,2-PDO	1,3-PDO	EG
Cu/MgO	8	52.2	95.1	–	1.5
	16	58.7	94.2	–	2
	24	66.2	93.9	–	1.9
	32	77.1	92.3	–	2.5
	40	85.2	90.9	–	3.1
Cu/ZrO_2	8	43.2	87.6	–	2.2
	16	51.4	87	–	2.4
	24	64.1	86	–	2.9
	32	74.6	85.5	–	3.2
	40	81.9	85	–	3.5

a) Reaction conditions: 10 wt% aqueous solution of glycerol 50.0 mL, 1.0 g of reduced catalyst, H_2 pressure 6.0 MPa, 180 °C.